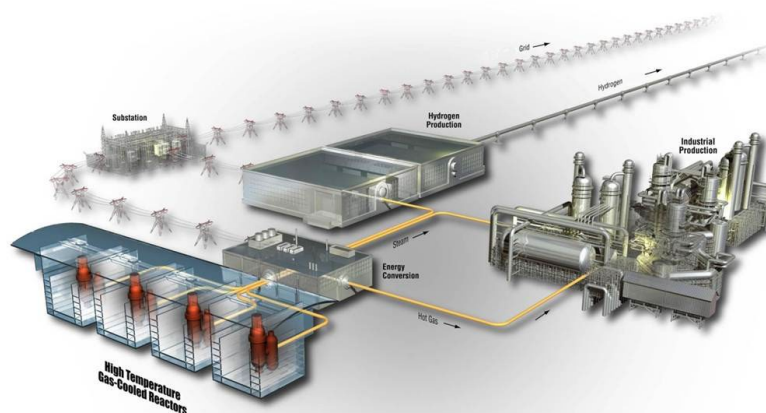# Initial Characterization of the Second A709 Commercial Heat

Changing the World's Energy Future

Ryann Bass
Idaho National Laboratory

Ting-Leung Sham
Idaho National Laboratory

INL
Idaho National Laboratory

Initial Characterization of the Second A709 Commercial Heat

Ryann Bass
Idaho National Laboratory
Ting-Leung Sham
Idaho National Laboratory

September 2022

Idaho National Laboratory
Advanced Reactor Technologies
Idaho Falls, Idaho 83415

http://www.art.inl.gov

Page intentionally left blank

INL ART Program

Initial Characterization of the Second A709 Commercial Heat

INL/RPT-22-69073
Revision 0

September 2022

Technical Reviewer: (Confirmation of mathematical accuracy, and correctness of data and appropriateness of assumptions.)

_____   9/8/2022
Michael D. McMurtrey   Date
ART Elevated-Temperature Metals Lead

Approved by:

M. Davenport   9/8/2022
_____   _____
Michael E. Davenport   Date
ART Project Manager

Travis Mitchell   9/8/2022
_____   _____
Travis R. Mitchell   Date
ART Program Manager

Michelle Sharp   9/8/2022
_____   _____
Michelle T. Sharp   Date
INL Quality Assurance

Page intentionally left blank

SUMMARY

In fiscal year 2021, Idaho National Laboratory (INL) received the second commercial heat of A709 in the plate-product form, heat 529900. The chemistry, microstructure, and mechanical properties of this heat were characterized. Heat 529900 met the chemistry and mechanical property requirements specified for UNS S31025 in American Society for Testing and Materials (ASTM) A213 and American Society of Mechanical Engineers SA-213 for seamless tube—from which A709 was derived. The microstructure of heat 529900 was comprised of equiaxed, recrystallized grains and elongated, unrecrystallized grains. The frequency of the unrecrystallized grains varied across the thickness of the plate with the highest frequency observed at the surface and none observed at the center. The equiaxed grain size of heat 529900 ranged from an ASTM grain size number 4 to an ASTM grain size number 6. The size of the equiaxed grains varied across the thickness of the plate with the coarsest grains located at the center of the plate. Additionally, the creep-fatigue properties of the second commercial heat were better than those of the first commercial heat.

Page intentionally left blank

ACKNOWLEDGEMENTS

Page intentionally left blank

CONTENTS

FIGURES

TABLES

ACRONYMS

ANL	Argonne National Laboratory
ART	Advanced Reactor Technologies
ASME	American Society of Mechanical Engineers
ASTM	American Society for Testing and Materials
ATI	Allegheny Technologies Incorporated
BPVC	Boiler and Pressure Vessel Code
DOE	U.S. Department of Energy
EAG	Evans Analytical Group
EBSD	electron backscatter diffraction
ESR	electroslag remelting
FR	Fast Reactors
FY	fiscal year
INL	Idaho National Laboratory
LTD	long transverse direction
MTR	material test report
NRC	U.S. Nuclear Regulatory Commission
ORNL	Oak Ridge National Laboratory
RD	rolling direction
SFR	sodium-cooled fast reactor
STD	short transverse direction
SS	stainless steel
U.S.	United States
w.r.t.	with respect to

Page intentionally left blank

Initial Characterization of the Second A709 Commercial Heat

1. MOTIVATION

President Biden's Executive Order 14008 issued a federal directive for the development of a plan to facilitate a carbon-zero electric-industry sector by 2035 (Exec. Order No. 14008 2021). Nuclear energy is one potential resource to satisfy this executive order. One of the leading advanced nuclear reactor concepts is the sodium-cooled fast reactor (SFR). Other needs not associated with this executive order but important for clean energy—such as the recycling of spent nuclear fuel—can also be attained with SFRs (Sham and Natesan 2017).

SFR commercialization is dependent upon these reactors being economically viable. A crucial aspect for this commercialization is qualification of advanced materials, which can reduce capital constructions costs. Although advanced materials are typically more expensive than traditional steels, they offer advantages that may ultimately lead to savings. Advanced materials may enable higher operating temperatures, which improve thermal efficiency and lead to increased power output. Additionally, advanced materials may offer longer design lifetimes, meaning components may not have to be replaced as regularly. Besides economic savings, advanced materials may offer improved safety margins, material reliability, and design flexibility (Sham and Natesan 2017).

A709, an austenitic stainless steel (SS), has been identified as an advanced material that would improve the viability of SFRs. A709 has better creep properties than 316H SS, the reference construction material for SFRs, but is not as expensive as nickel-based alloys usually used at high temperatures. This enables the construction of thinner walled components which reduces construction costs. A709 has an improved resistance to thermal gradients as compared to 316H SS. This eliminates the need for expensive add-on hardware required for construction with 316H SS which further reduces construction costs. Potential SFR components to be constructed with A709 are the reactor vessel, piping, core supports, intermediate heat exchanger, and compact heat exchanger. The compact heat exchanger could link the SFR to a supercritical carbon dioxide Brayton energy conversion system as one possible application (Sham and Natesan 2017).

In the United States (U.S.), the U.S. Nuclear Regulatory Commission (NRC) licenses and regulates nuclear reactors and nuclear reactor designs. Section III, Division 5 of the American Society of Mechanical Engineers (ASME) Boiler and Pressure Vessel Code (BPVC) provides design rules for elevated-temperature nuclear construction (ASME 2021a). It is under consideration by NRC for endorsement (Thomas 2018; Nuclear Regulatory Commission 2022) which would increase regulatory efficiency. Advanced reactor developers can design high-temperature reactor components to the rules of Section III, Division 5 to reduce regulatory risk. A709 is currently not qualified in Section III, Division 5 of the ASME BPVC. A program comprised of a collaboration between three U.S. Department of Energy (DOE) national laboratories—Argonne National Laboratory (ANL), Idaho National Laboratory (INL), and Oak Ridge National Laboratory (ORNL)—is in progress to qualify A709 in Section III, Division 5 of the ASME BPVC through multiple Code Cases. These Code Cases require putting together data packages that involve conducting tests to collect A709 data from which the design parameters for A709 will be established.

A plan for developing the data packages needed to qualify A709 in Section III, Division 5 of the ASME BPVC was formulated. This plan considered the needs of both the ASME BPVC and NRC on components construction and reactor licensing and operations (Sham and Natesan 2017). This includes Nonmandatory Appendix HBB-Y in Section III, Division 5 of the ASME BPVC, which provides guidelines for qualifying new materials. Nonmandatory Appendix HBB-Y specifies the data package for qualifying new materials must be comprised of data from a minimum of three heats, which needs to encompass the composition range of the components to be used in service (ASME 2021a).

The first commercial heat of A709 was procured in fiscal year (FY) 2017 from Electralloy/G.O. Carlson, heat 58776. This heat has been characterized and Code Case testing is in progress (Natesan et al. 2017; Sham et al. 2022; Rupp et al. 2021; Wang, Hou, and Sham 2021; Zhang, Sham, and Li 2021; Bass and Sham 2022). In FY 2020, INL placed a purchase order with Allegheny Technologies Incorporated (ATI) Flat Rolled Products to procure the second commercial heat of plate A709 (Wright 2020). The A709 plates, heat 529900, were delivered by ATI in March 2021. The purpose of this report is to provide an initial characterization of heat 529900. This characterization includes chemistry, microstructure, and mechanical properties.

2. EXPERIMENTAL METHODOLOGY

2.1 Second Commercial Heat of Plate A709

The second commercial heat of the plate-product form of A709 was procured from ATI. A total of nine plates were fabricated. All of the plates were from the same master argon oxygen decarburization heat identified as heat 529900. Heat 529900 was comprised of three sub-heats which correlates to the electroslag remelting (ESR) final processing step that was used for all nine plates. In other words, ESR was conducted three times for heat 529900 with each sub-heat comprised of three plates. Of the nine plates that comprised heat 529900, eight were hot-rolled and solution-annealed; six of these eight plates were nominally 44 mm (1.75 in.) thick and the remaining two were nominally 51 mm (2.0 in.) thick. The solution anneal was conducted at a minimum of 1149°C (2100°F). The remaining plate was nominally 44 mm (1.75 in.) thick and delivered in the hot-rolled condition. In this report, the plate axes are referred to as the rolling direction (RD), long transverse direction (LTD), and short transverse direction (STD). These correspond to the length, width, and thickness of the plate, respectively.

2.2 Chemical Verification

A chemical verification of sub-heats one and two of heat 529900 was conducted by Eurofins Evans Analytical Group (EAG) Laboratories. Glow discharge mass spectrometry, instrumental gas analysis, and inductively coupled plasma optimal emission spectrometry were conducted for both sub-heats.

2.3 Microstructural Characterization

Microstructure was characterized using a combination of light optical microscopy, scanning electron microscopy, and electron backscatter diffraction (EBSD). A Keyence VHX-6000 light optical microscope and FEI Quanta FEG 650 scanning electron microscope were used. EBSD data was collected with the TEAM™ software from EDAX using a 2 μm step size. EBSD data was processed using MTEX, a free toolbox in Matlab. EBSD data with a confidence index less than or equal to 0.1 was removed from analysis. A misorientation between neighboring pixels larger than 5° defined a grain boundary. Grains were required to be comprised of a minimum of five pixels.

Specimens were extracted from plates CG05455 and CG05453. These plates had a nominal thickness of 44 mm (1.75 in.) and 51 mm (2.0 in.), respectively. Both plates were in the solution-annealed condition. Specimens were extracted from the plates in the following locations: 1) from the middle of the plate with respect to (w.r.t.) the RD and 2) from both the middle and edge of the plate w.r.t. the LTD. Characterization was conducted on the RD-STD plane for the entire thickness of the plate. Specimens were prepared using standard grinding and polishing techniques. Electroetching with a 10% oxalic acid solution and 2.2 V for 10 to 30 seconds successfully revealed grain boundaries for light optical microscopy characterization.

Grain size was measured using the comparison procedure in accordance with American Society for Testing and Material (ASTM) standard E112-13, "Standard Test Methods for Determining Average Grain Size" (ASTM 2013). Grain size was measured across the entire span of the plate thickness in the manner shown in Figure 1. Each dot represents the general location where grain size was characterized. This approach was a consequence of specimen preparation size limitations.
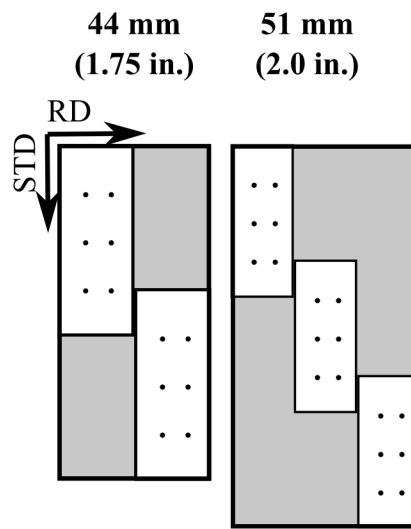
Figure 1. Schematic illustrating the approach to characterize the grain size of the 44 mm (1.75 in.) and 51 mm (2.0 in.) thick plates. Each dot represents the general location where grain size was characterized.

2.4 Mechanical Testing

2.4.1 Tensile

Room-temperature tensile tests were conducted in accordance with PLN-3349, "Tensile Testing," and ASTM E8, "Standard Test Methods for Tension Testing of Metallic Materials" (INL 2009; ASTM 2021a). A cylindrical test specimen geometry with a 6.35 mm (0.250 in.) minimum diameter and a reduced parallel section that was at minimum 31.75 mm (1.250 in.) was used. The specimens were tested to failure using an electromechanical test frame. The yield strength, tensile strength, elongation, and reduction in area were measured. Yield strength was determined using the offset method with an offset of 0.2%. Elongation was calculated from elongation-after-fracture measurements. Prior to testing, the gauge was marked with two indentations that were 25.4 mm (1 in.) apart. The distance between the indentations was measured with calipers post-test.

Tensile specimens were extracted from plates CG05455 and CG05453. These plates had a nominal thickness of 44 mm (1.75 in.) and 51 mm (2.0 in.), respectively. Both plates were in the solution-annealed condition. Specimens were extracted from the plates in the following locations: (1) from the middle of the plate w.r.t. the RD, (2) from both the middle and edge of the plate w.r.t. the LTD, and (3) at one-quarter and three-quarters of the plate thickness w.r.t. the STD. Tensile tests were conducted with the longitudinal direction of the specimen parallel and perpendicular to the RD. For this report, these specimen orientations are referred to longitudinal and transverse, respectively.

2.4.2 Hardness

Vickers hardness was measured using a LECO LM247AT hardness tester. Hardness was measured in accordance with ASTM standard E92-17, "Standard Test Methods for Vickers Hardness and Knoop Hardness of Metallic Materials," and ASTM E384-17, "Standard Test Method for Microindentation Hardness of Materials" (ASTM 2017a; 2017b). A 300 gf indentation test force with a 13-second dwell time was used.

Hardness was measured on specimens extracted from plates CG05455 and CG05453. These plates had a nominal thickness of 44 mm (1.75 in.) and 51 mm (2.0 in.), respectively. Both plates were in the solution-annealed condition. Specimens were extracted from the plates in the following locations: 1) from the middle of the plate w.r.t. the RD and 2) from both the middle and edge of the plate w.r.t. the LTD.

Hardness was measured on the RD-STD plane. The hardness was measured every 500 μm across the span of the plate thickness. This was carried out three times.

2.4.3 Creep-fatigue

A creep-fatigue test was conducted in accordance with ASTM E2714-13, "Standard Test Method for Creep-Fatigue Testing," and ASTM E606/E606M-12, "Standard Test Method for Strain-Controlled Fatigue Testing" (ASTM 2020, 2012). The test was also conducted in accordance with PLN-3346, "Creep Fatigue Testing" (INL 2017). A cylindrical test specimen with a minimum diameter of 7.49 mm (0.29 in.) was used. The extensometer gauge length was 12 mm (0.47 in.). The test was strain-controlled with a 30-minute hold at the peak tensile strain. The strain was fully reversed (R = -1) with a total strain range of 1.0%. R is the ratio of the minimum strain over the maximum strain. The strain rate was 10^{-3} s^{-1}. The test was conducted at 650°C (1202°F).

The creep-fatigue specimen was extracted from plate CG05455 which was nominally 44 mm (1.75 in.) thick in the solution-annealed condition. The specimen was extracted from the middle of the plate w.r.t. the RD and LTD and at one-quarter or three-quarters the plate thickness w.r.t. the STD. The longitudinal direction of the specimen was parallel to the RD of the plate.

3. RESULTS AND DISCUSSION

3.1 Chemistry

The chemical composition of heat 529900 is in accordance with the chemistry requirements specified in ASTM A213 and ASME SA-213 for UNS S31025. Both specifications are entitled "Standard Specification for Seamless Ferritic and Austenitic Alloy-Steel Boiler, Superheater, and Heat Exchanger Tubes" (ASTM 2021b; ASME 2021b). UNS S31025 is the designation for NF709 which A709 was derived from.

Table 1 shows the chemistry of heat 529900 and the requirements specified in ASTM A213 and ASME SA-213 for UNS S31025. Only elements listed in these specifications or the statement of work to procure heat 529900 are included in Table 1 (ASTM 2021b; ASME 2021b; Wright 2020). This table includes the chemistry reported in the material test report (MTR) provided by ATI for the three sub-heats. An independent verification of the chemical composition of heat 529900 performed by Eurofins EAG Laboratories is also included in Table 1.

Table 1. Chemical composition, in weight percent, of heat 529900 reported in the MTR and by Eurofins EAG Laboratories. The chemistry requirements specified in ASTM A213 and ASME SA-213 for UNS S31025 are also provided (ASTM 2021; ASME 2021b).

Sub heat	Source	C	Mn	Si	P	S	Cr
1	MTR	0.08	0.9	0.39	0.003	< 0.001	19.9
	Eurofins	0.078	0.89	0.3	0.0034	0.000082	20.0
2	MTR	0.08	0.9	0.35	0.004	< 0.001	20.0
	Eurofins	0.078	0.9	0.3	0.002	0.000062	20.0
3	MTR	0.08	0.9	0.37	0.003	< 0.001	19.9
	UNS S31025	0.10 max	1.50 max	1.00 max	0.030 max	0.030 max	19.5 – 23.0

Sub heat	Source	Ni	Mo	N	Nb	Ti	Cu
1	MTR	24.6	1.5	0.15	0.17	< 0.01	0.06
	Eurofins	25.0	1.48	0.14	0.19	0.00067	0.043
2	MTR	24.6	1.5	0.16	0.17	< 0.01	0.07
	Eurofins	25.2	1.48	0.14	0.22	0.00078	0.043
3	MTR	24.5	1.5	0.15	0.17	0.01	0.06
	UNS S31025	23.0 – 26.0	1.0 – 2.0	0.10 – 0.25	0.10 – 0.40	0.20 max	—

Sub heat	Source	Co	Al	B	Fe		
1	MTR	0.02	0.02	0.004	Bal.	—	—
	Eurofins	0.019	0.036	0.0046	52.6	—	—
2	MTR	0.02	0.01	0.005	Bal.	—	—
	Eurofins	0.019	0.014	0.0049	52.4	—	—
3	MTR	0.02	0.04	0.004	Bal.	—	—
	UNS S31025	—	—	0.002 – 0.010	—	—	—

Bal. = Balance

3.2   Microstructure

The microstructure of ATI heat 529900 is comprised of a combination of equiaxed, recrystallized grains and elongated, uncrystallized grains. The density of the unrecrystallized grains was greatest at the surface of the plates w.r.t. the STD. Unrecrystallized grains were not observed to be present at the middle of the plate w.r.t. the STD. The density of the unrecrystallized grains were observed to be higher in the specimens from the 51 mm (2.0 in.) thick plate compared to the specimens from the 44 mm (1.75 in.) thick plate. Representative light optical microscopy images of the microstructure of the 44 mm (1.75 in.) and 51 mm (2.0 in.) thick plates are shown in Figure 2 and Figure 3, respectively. The elongated grains were determined to be unrecrystallized grains based on the large amounts of deformation observed in these grains. This is shown in Figure 4 and Figure 5 where the significant color variations in the elongated grains indicate significant variations in crystallographic orientation and consequently large amounts of deformation. This is in stark comparison to the equiaxed grains in Figure 4 and Figure 5 which are uniformly colored indicating these grains do not contain much deformation.
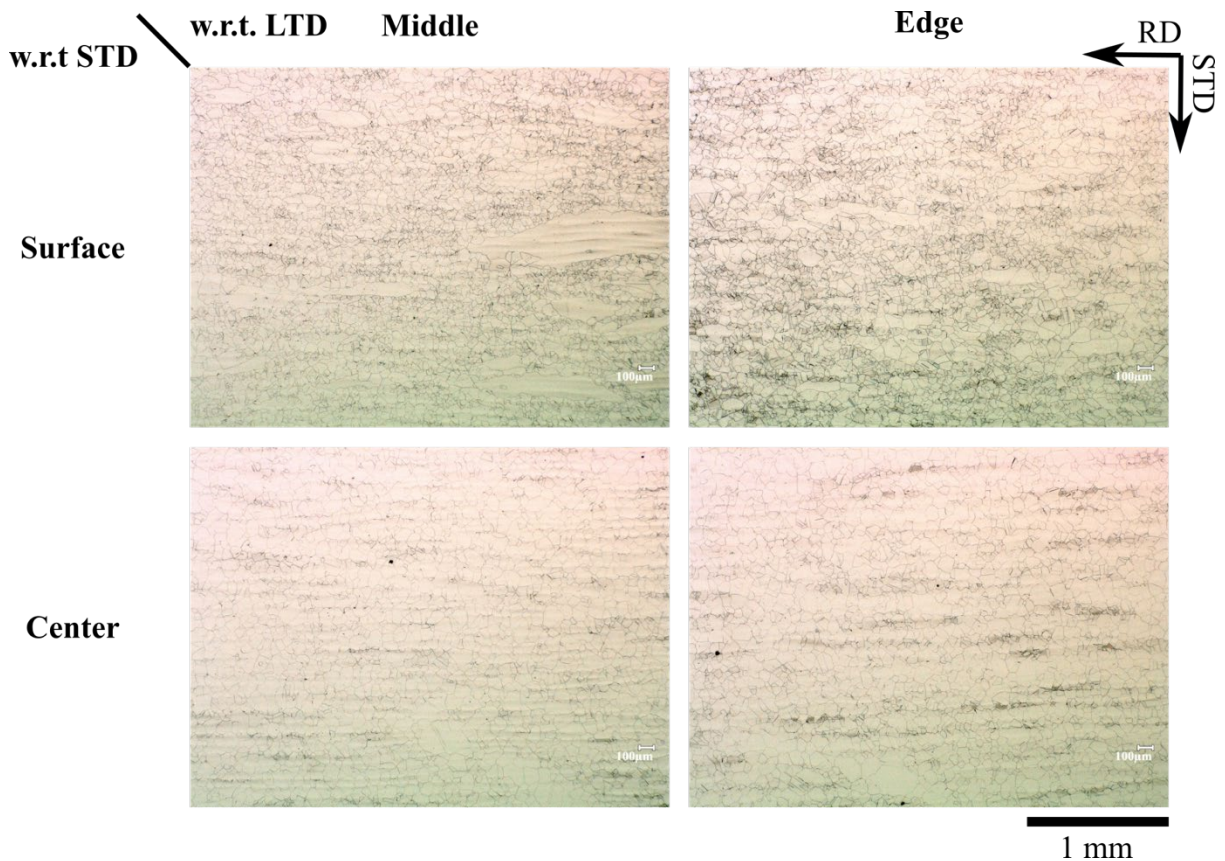

Figure 2. Representative light optical microscopy images of the microstructure of the 44 mm (1.75 in.) thick plate.

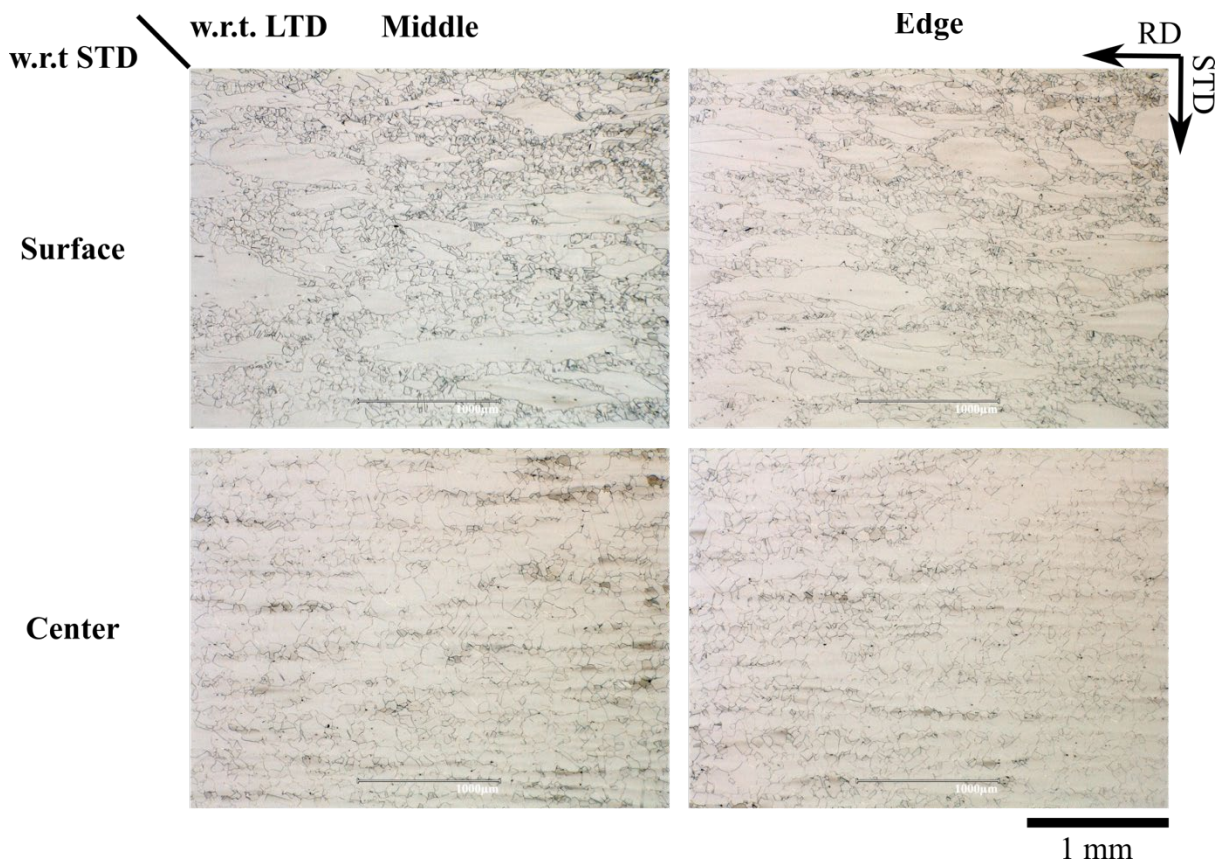Figure 3. Representative light optical microscopy images of the microstructure of the 51 mm (2.0 in.) thick plate.
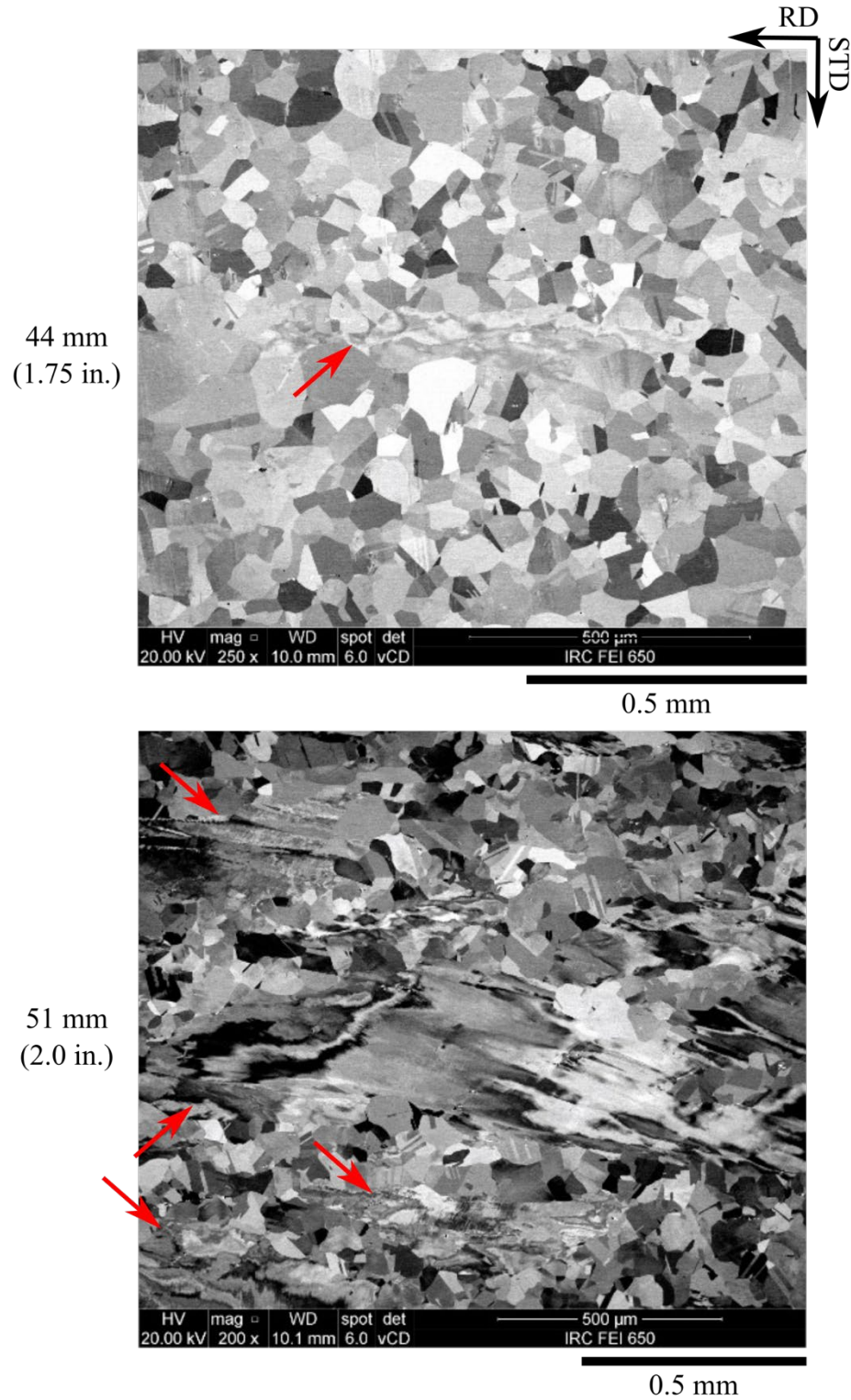
Figure 4. Back-scattered-electron images from the middle of the plate w.r.t. the LTD. The top and bottom image are for the plates that are 44 mm (1.75 in.) and 51 mm (2.0 in.) thick, respectively. Instances of the elongated, unrecrystallized grains are highlighted with the red arrows.
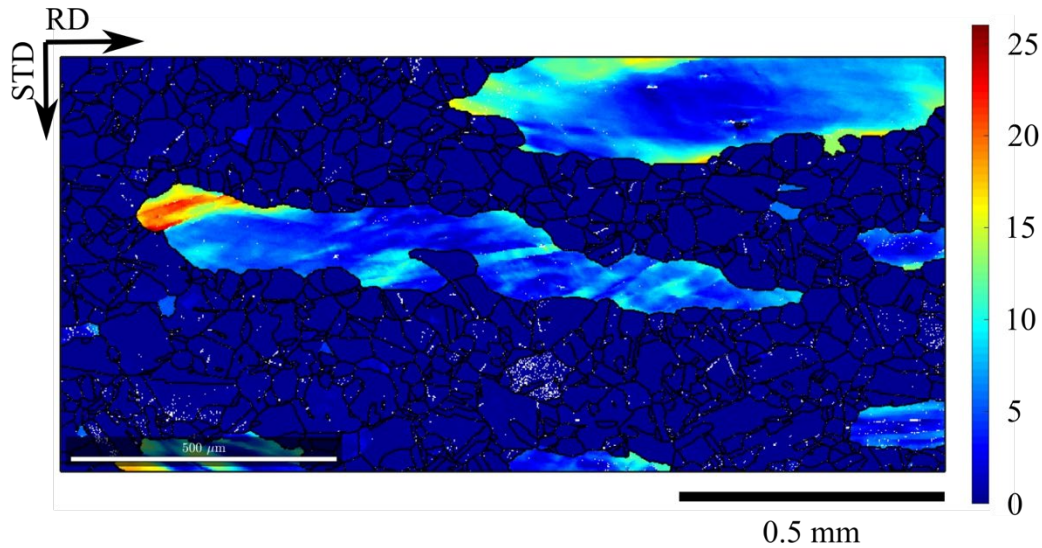
Figure 5. Reference orientation deviation map determined from EBSD data collected from the middle of the 51 mm (2.0 in.) thick plate with respect to the LTD.

The equiaxed grain size of heat 529900 ranged from an ASTM grain size number 4 to an ASTM grain size number 6. The size of the equiaxed grains was observed to vary across the STD with the coarsest equiaxed grains located at the center of the plate w.r.t. the STD and the smallest equiaxed grains located at the surface of the plates w.r.t. the STD, as shown in Figure 6. The area of the coarsest equiaxed grains w.r.t. the STD was observed to bigger at the middle of the plate w.r.t. the LTD compared to the edge of the plate w.r.t. the LTD. The equiaxed grains in the 51 mm (2.0 in.) thick plate were coarser than the grains in the 44 mm (1.75 in.) thick plate. The grain size of the unrecrystallized grains was not characterized. The grain size of the equiaxed grains was not characterized if the density of the unrecrystallized grains was too extensive to permit enough equiaxed grains to be in the field of view for characterization.
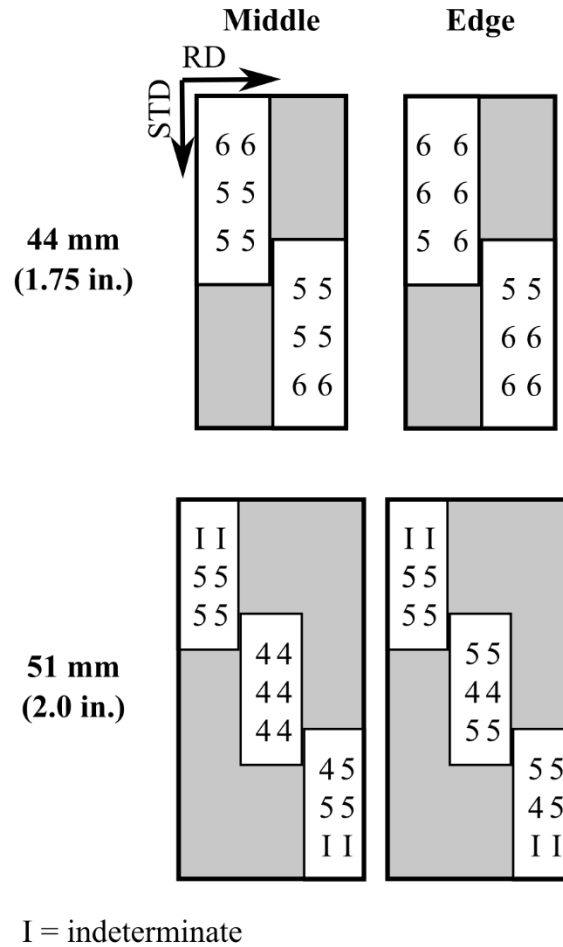
Figure 6. Grain size at the middle and edge of the 44 mm (1.75 in.) and 51 mm (2.0 in.) thick plates w.r.t. the LTD.

3.3   Mechanical Properties

3.3.1   Tensile

ATI heat 529900 exceeded the minimum room-temperature tensile requirements specified in ASTM A213 and ASME SA-213 for UNS S31025 (ASTM 2021b; ASME 2021b). This is demonstrated in Table 2 which shows the yield strength, tensile strength, elongation, and reduction in area for the specimens sampled from heat 529900. Table 2 also includes the minimum requirements specified in ASTM A213 and ASME SA-213 for UNS S31025 (ASTM 2021b; ASME 2021b).

Table 2. Room-temperature tensile properties of specimens sampled from heat 529900. The minimum room-temperature tensile properties specified in ASTM A213 and ASME SA-213 for UNS S31025 are also provided (ASTM 2021b; ASME 2021b).

Plate	Nominal Thickness (mm)	Plate Location	Test Orientation	Yield Strength[1] (MPa)	Tensile Strength (MPa)	Elongation (%)	Reduction in Area (%)
CG05455	44	Middle	Transverse	299	695	56	72
		Edge	Transverse	318	696	55	71
			Longitudinal	317	698	57	72
CG05453	51	Middle	Transverse	313	690	55	72
			Longitudinal	310	687	57	73
		Edge	Transverse	327	682	55	71
			Longitudinal	328	690	55	73
UNS S31025 minimum requirements				270	640	30	Not Specified

[1]Offset = 0.2%

3.3.2 Hardness

ATI heat 529900 meets the hardness requirements specified in ASTM A213 and ASME SA-213 for UNS S31025 (ASTM 2021b; ASME 2021b). This is shown in Figure 7 for the 44 mm (1.75 in.) thick plate. The square represents the average hardness of the three measurements while the top and bottom error bars correspond to the maximum and minimum hardness measured, respectively. From Figure 7, it is apparent that the hardness of the plate did not vary significantly w.r.t. the LTD. The hardness did vary slightly w.r.t. the STD with a higher hardness observed at the surface compared to the center. The same trends were observed in the 51 mm (2.0 in.) thick plate.
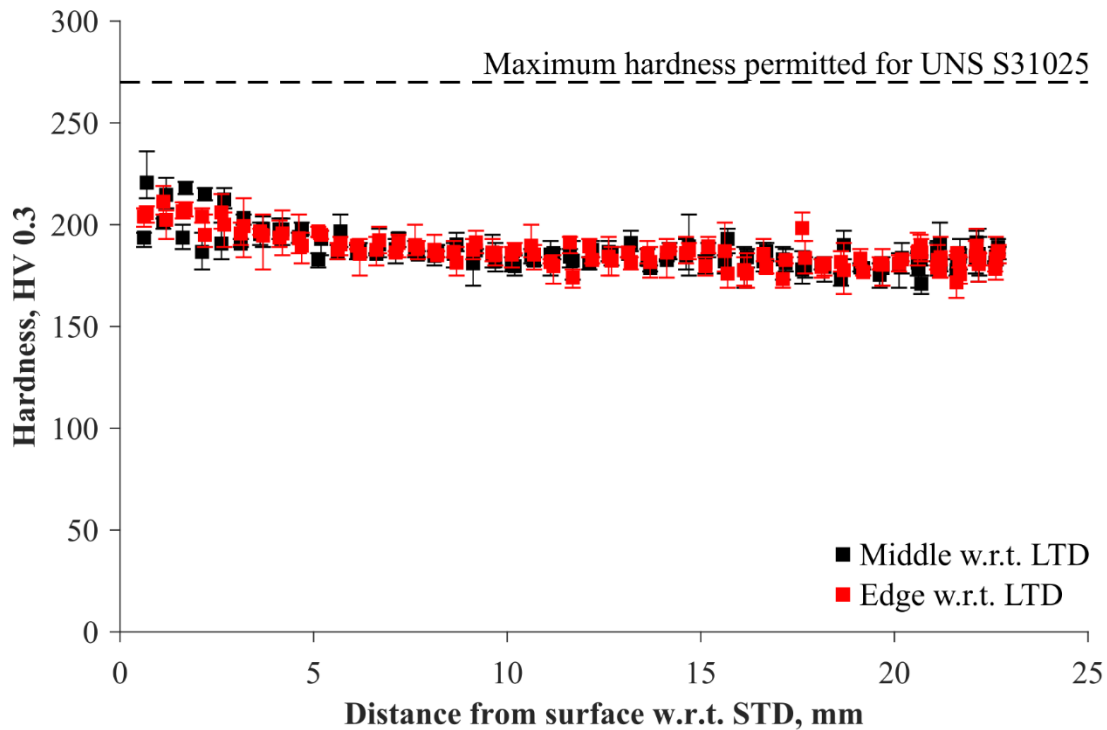
Figure 7. Hardness as a function of distance from the surface of the 44 mm (1.75 in.) thick plate w.r.t. the STD for specimens extracted from the middle and edge of the plate w.r.t. the LTD. The maximum permissible hardness for UNS S31025 specified in ASTM A213 and ASME SA-213 is shown by the dashed horizontal line (ASTM 2021; ASME 2021b).

3.3.3   Creep-fatigue

The creep-fatigue properties of ATI heat 529900 were better than the creep-fatigue properties of Carlson heat 58776. This is shown in Figure 8 where the specimen from the ATI heat had a greater number of cycles to failure compared to the three specimens tested at the same conditions from the Carlson heat. The Carlson specimens were extracted from a plate with the ESR final processing step that was solution-annealed at 1150°C (2102°F). The peak stress for a given cycle was similar for the specimens from the ATI and Carlson heats. One difference was that the ATI specimen exhibited slower cyclic hardening compared to the Carlson specimens at the start of the test. Figure 9 and Figure 10 show the hysteresis loops and stress relaxation curves at the midlife cycle for the four tests shown in Figure 8. From these figures, it should be highlighted that the specimen from the ATI heat relaxed faster compared to the specimens from the Carlson heat.
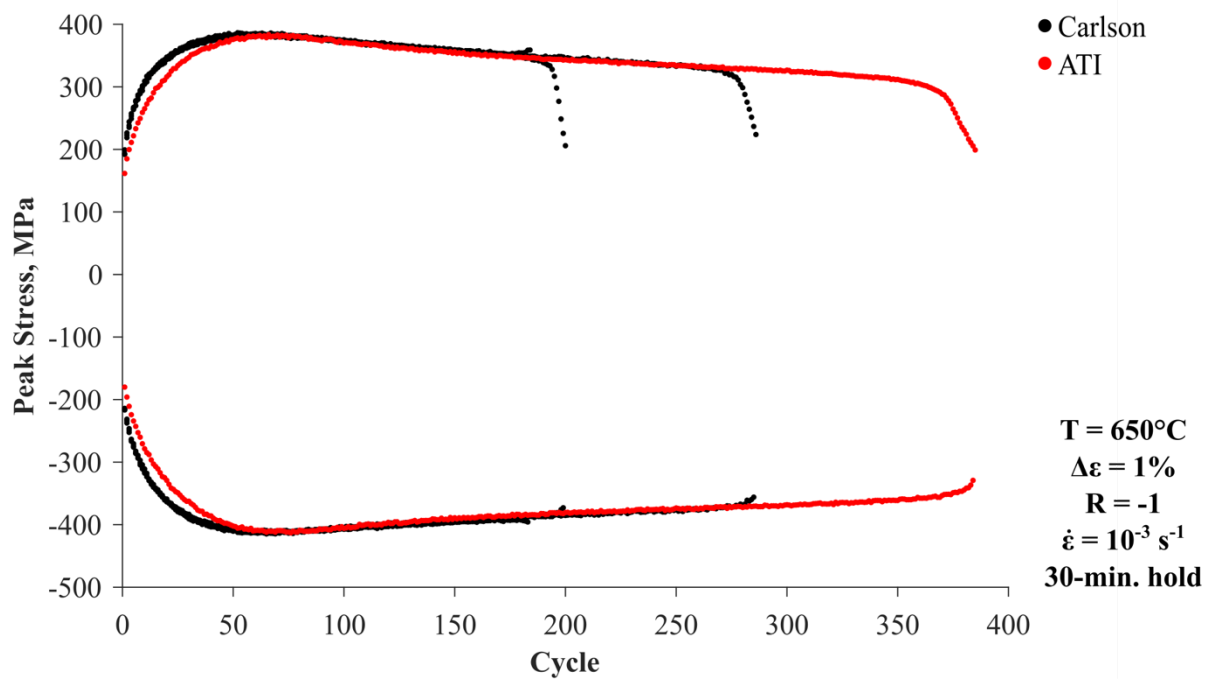
Figure 8. Peak stress as a function of cycle for the Carlson and ATI commercial heats of A709 in the plate-product form. The specimens were strain-controlled creep-fatigue tested at 650°C (1202°F) with a 30-minute tensile hold. The total strain range was 1% and fully reversed.
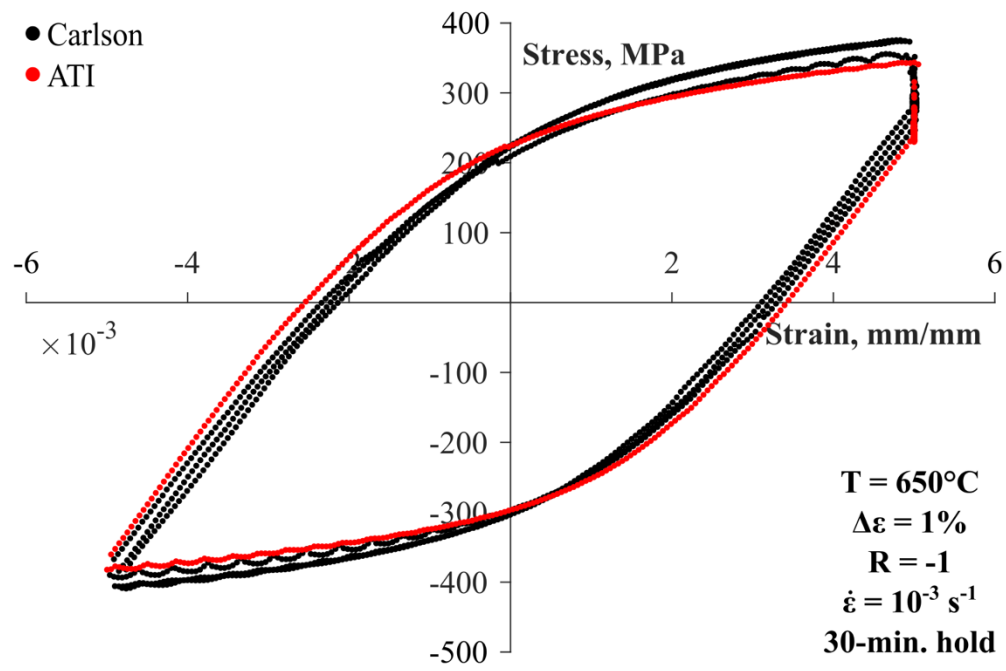
Figure 9. Stress as a function of strain during the midlife cycle for the Carlson and ATI commercial heats of A709 in the plate-product form. The specimens were strain-controlled creep-fatigue tested at 650°C (1202°F) with a 30-minute tensile hold. The total strain range was 1% and fully reversed.
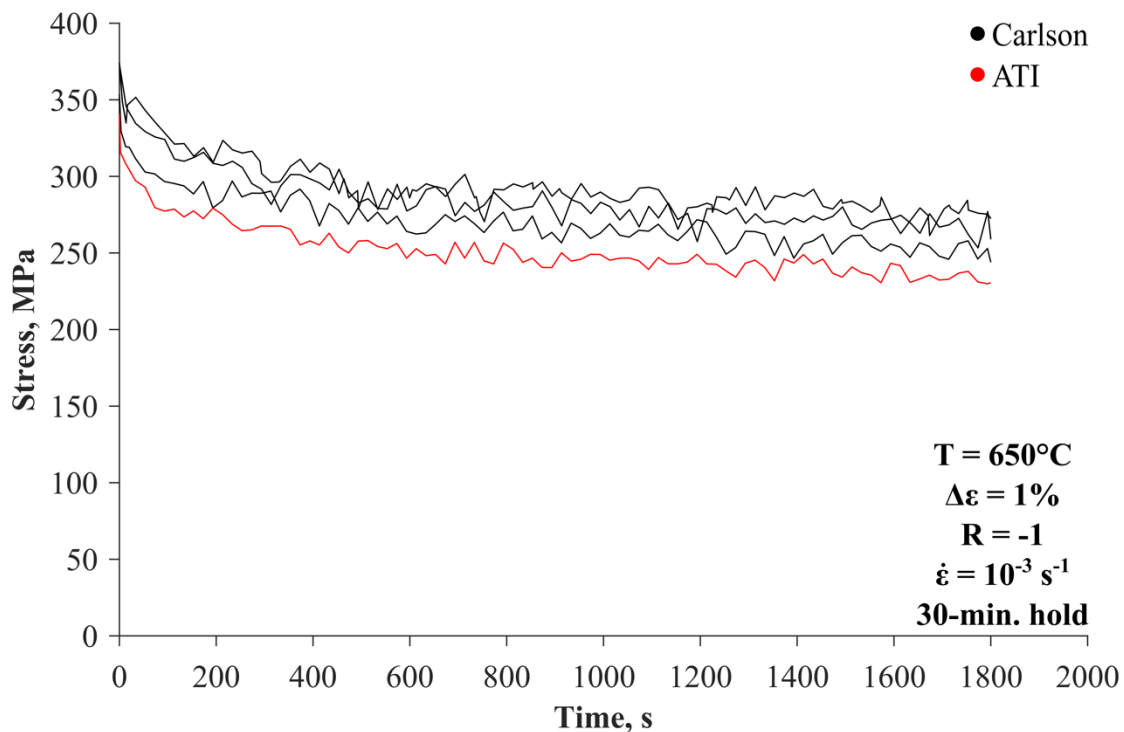
Figure 10. Stress as a function of time during the midlife cycle 30 minute (1800 s) hold at the peak tensile strain for the Carlson and ATI commercial heats of A709 in the plate-product form. The specimens were strain-controlled creep-fatigue tested at 650°C (1202°F) with a 30-minute tensile hold. The total strain range was 1% and fully reversed.

4. SUMMARY AND ONGOING WORK

In FY 2021, INL received the second commercial heat of A709 in the plate-product form, heat 529900. The chemistry, microstructure, and mechanical properties of this heat were characterized. Heat 529900 met the chemistry and mechanical property requirements specified for UNS S31025 in American Society for Testing and Materials (ASTM) A213 and ASME SA 213 for seamless tube from which A709 was derived. The microstructure of heat 529900 was comprised of equiaxed, recrystallized grains and elongated, unrecrystallized grains. The frequency of the unrecrystallized grains varied across the thickness of the plate with the highest frequency observed at the surface and none observed at the center. The equiaxed grain size of heat 529900 ranged from an ASTM grain size number 4 to an ASTM grain size number 6. The size of the equiaxed grains varied across the thickness of the plate with the coarsest grains located at the center of the plate. Additionally, the creep-fatigue properties of the second commercial heat were better than those of the first commercial heat.

In FY 2021, INL placed a purchase order with ATI to procure the third commercial heat of plate A709. The A709 plates, heat 530843, were delivered by ATI to ORNL in April 2022. This heat is currently being sectioned into smaller pieces by waterjet cutting. An initial characterization of this heat needs to be conducted in a similar manner as to what was performed for the second commercial heat.

15

6. REFERENCES

ASME International. 2021a. "Section III, Division 5: Rules for Construction of Nuclear Facility Components, High Temperature Reactors." In *ASME Boiler and Pressure Vessel Code: An International Code*. New York, NY: ASME.

ASME International. 2021b. "Standard Specification for Seamless Ferritic and Austenitic Alloy-Steel Boiler, Superheater, and Heat Exchanger Tubes." ASME SA-213/SA-213M. New York, NY.

ASTM International. 2012. "Standard Test Method for Strain-Controlled Fatigue Testing." ASTM E606/E606M-12. West Conshohocken, PA.

ASTM International. 2013. "Standard Test Methods for Determining Average Grain Size." ASTM E112-13. West Conshohocken, PA.

ASTM International. 2017a. "Standard Test Methods for Vickers Hardness and Knoop Hardness of Metallic Materials." ASTM E92-17. West Conshohocken, PA.

ASTM International. 2017b. "Standard Test Method for Microindentation Hardness of Materials." ASTM E384-17. West Conshohocken, PA.

ASTM International. 2020. "Standard Test Method for Creep-Fatigue Testing." ASTM E2714-13 (Reapproved 2020). West Conshohocken, PA.

ASTM International. 2021a. "Standard Test Methods for Tension Testing of Metallic Materials." ASTM E8/E8M-21. West Conshohocken, PA.

ASTM International. 2021b. "Standard Specification for Seamless Ferritic and Austenitic Alloy-Steel Boiler, Superheater, and Heat-Exchanger Tubes." ASTM A213/A213M-21a. West Conshohocken, PA.

Bass, Ryann and Ting-Leung Sham. 2022. "Interim Creep, Fatigue and Creep-Fatigue Data from FY 2022 INL Testing of A709 with Precipitation Treatment for ASME Code Case Data Package." INL/RPT-22-68982 Rev000, Idaho National Laboratory.

Executive Order No. 14,008. 2021. 3 C.F.R 7624. "Tackling the Climate Crisis at Home and Abroad." January 27, 2021.

Idaho National Laboratory. 2009. "Tensile Testing." PLN-3349 Revision 0, Idaho National Laboratory.

Idaho National Laboratory. 2017. "Creep Fatigue Testing." PLN-3346 INL/MIS-10-18953-Rev009, Idaho National Laboratory.

Natesan, Krishnamurti, Xuan Zhang, Ting-Leung Sham, and Hong Wang. 2017. "Report on the Completion of the Procurement of the First Heat of Alloy 709." ANL-ART-89, Argonne National Laboratory. https://doi.org/10.2172/1364649.

Nuclear Regulatory Commission. 2022. "Acceptability of ASME Code Section III, Division 5, High Temperature Reactors." NRC-2021-0117. 87 Fed. Reg. 11,490. March 1, 2022.

Rupp, Ryann, Yanli Wang, Xuan Zhang, and Ting-Leung Sham. 2021. "Integrated FY-2021 Elevated-Temperature Mechanical-Testing Results for Alloy 709 Code Case." INL/EXT-21-64314-REV000, Idaho National Laboratory.

Sham, Ting-Leung and Krishnamurti Natesan. 2017. "Code Qualification Plan for an Advanced Austenitic Stainless Steel, Alloy 709, for Sodium Fast Reactor Structural Applications." International Conference on Fast Reactors and Related Fuel Cycles: Next Generation Nuclear for Sustainable Development (FR17), Yekaterinburg, Russia, IAEA-CN-245-74.

Sham, Ting-Leung, Yanli Wang, Ryann Bass, and Xuan Zhang. 2022. "A709 Qualification Plan Update and Mechanical Properties Data Assessment." INL/RPT-22-67641, Idaho National Laboratory.

Thomas, Brian E. 2018. "NRC Response to ASME Letter of Request for NRC Endorsement of ASME Boiler and Pressure Vessel Code, Section III, Division 5". ML18211A571, United States Nuclear Regulatory Commission.

Wang, Yanli, Peijun Hou, and Ting-Leung Sham. 2021. "Report on FY 2021 Creep, Fatigue, and Creep Fatigue Testing of Alloy 709 Base Metal at ORNL." ORNL/TM-2021/2120, Oak Ridge National Laboratory.

Wright, Richard N. 2020. "Report Documenting Activity for Second Alloy 709 Commercial Heat." INL/EXT-20-59880-Rev000, Idaho National Laboratory.

Zhang, Xuan, Ting-Leung Sham, and Meimei Li. 2021. "FY21 Status Report on Creep Rupture Testing at ANL to Support the Development of Alloy 709 Code Case." ANL-ART-231, Argonne National Laboratory. https://doi.org/10.2172/1810715.